The following publication R. Qi, Y. P. Du and M. Chen, "A Full-Wave PEEC Model of Thin-Wire Structures Above the Lossy Ground," in IEEE Transactions on Electromagnetic Compatibility, vol. 62, no. 5, pp. 2055-2064, Oct. 2020 is available at https://doi.org/10.1109/TEMC.2019.2949346.

A Full-wave PEEC Model of Thin-wire Structures above the Lossy Ground

Ruihan Qi, Y. Du[1] and Mingli Chen

Dept. of Building Services Engineering, the Hong Kong Polytechnic University

Hung Hom, Kowloon, Hong Kong

[1]ya-ping.du@polyu.edu.hk

Abstract — **This paper addresses a full-wave PEEC model of wire structures above a lossy ground for lightning transient analysis. The PEEC model is formulated with dyadic Green's functions. An equivalent circuit is derived for the first time by including correction terms arising from the lossy ground. Circuit parameters are expressed using Sommerfeld integrals, which can be evaluated numerically and be presented with lookup tables. The low-frequency model of the lossy ground is derived, and is depicted using the the mirror image of source elements, similar to the case of a perfect ground. The comparison of circuit parameters calculated with this model and the Sommerfeld integrals is made. The proposed method is validated numerically with the numerical computation code (NEC2) in the frequency domain, and the FDTD method in the time domain. Good agreements are observed. The proposed method is then applied to analyze lightning transients in a wire structure over the lossy ground. It is concluded that the lossy ground can be substituted with the low-frequency model for transient analysis. The computational burden in the time-domain simulation can be significantly relieved.**

Keywords — **lightning, transient, PEEC, lossy ground, Green's function**

1. INTRODUCTION

Lightning transients in multi-conductor systems are a long-standing issue. Such conductors can be found in electric power systems, communication systems, electrified railway as well as buildings. They may run in an arbitrary direction, and are inter-connected to form a three-dimensional wire structure over a lossy ground. When a system is struck by lightning, a lightning current will be generated in the structure. For effective protection against lightning, it would be necessary to have appropriate procedures for modeling and evaluation of lightning transients in the structure.

Transient analysis in transmission lines has been extensively addressed in the literature [1]. These lines are modeled with distributed circuits. Line parameters of these circuits are determined by geometries of the transmission lines and parameters of the lossy ground. The effect of finite ground parameters has been well addressed, and various formulas were presented and summarized in [2]. In an indirect lightning strike, lightning transients in a transmission line are generated by electromagnetic coupling. The formulations of induced voltages in a horizontal line over the lossy ground have been addressed as well [3-8]. These approaches have been widely used in addressing lightning transients in the overhead lines. However, they are difficult to apply for a set of arbitrarily-orientated short conductors over the lossy ground.

The partial element equivalent circuit (PEEC) method is the one for modeling 3D interconnected thin-wire structures [9-10]. It is derived from a mixed potential integral equation, and transforms an electromagnetic problem into the circuit domain [11-13]. Recently this method has been applied to address both transient current and voltage in a variety of structures with arbitrarily-orientated lines [14-20] and others [21-24]. In many cases a perfectly conducting ground or the complex plane method was adopted to derive circuit parameters [14-15,25]. In [26] a full-wave PEEC formulation using Green's functions was presented for a layered dielectric structure with perfect ground slabs at its two ends. These studies have made significant contributions to the development of PEEC theory and its applications. As the effect of the lossy ground was not taken into account appropriately, a significant error could yield.

It is noted in [27] that a PEEC model of vertical lines over a lossy ground was derived using Green's functions. This paper presents a full-wave PEEC formulation for arbitrary-orientated conductors over a lossy ground for lightning transient analysis. Section II describes the detail of the proposed PEEC formulation. The effect of a lossy ground is modeled using dyadic Green's functions. An equivalent circuit is presented by taking into account correction terms arising from the presence of the lossy ground. In Section III, general expressions of circuit parameters are presented using Sommerfeld integrals, which can be evaluated numerically. Closed-formulas of circuit parameters for two simple ground models are derived. Circuit parameters of sample wires over the lossy ground are evaluated, and comparisons with the low-frequency model of the lossy ground are made in this section. Section IV presents the comparison of the current responses calculated with the proposed method and numerical computation code (NEC2) [28]. Comparison with the finite-difference and finite-element method (FDTD) in the time domain is presented as well. Finally, in Section V, the proposed method is applied to evaluate lightning transients in a wire structure over the lossy ground. The results calculated with simple ground models are also presented for comparison.

II. FULL-WAVE PEEC FORMULATION

Auxiliary potentials are often used to simplify the mathematical analysis of Maxwell's equations. Those are the magnetic vector potential $\boldsymbol{A}$ and the electric scalar potential ϕ. They satisfy the following equation at point r on the conductor surface [29],

$$\boldsymbol{E}(r)+j\omega\boldsymbol{A}(r)=-\nabla\phi(r) \tag{1}$$

where $\boldsymbol{E}$ is the electric field on the conductor surface, and ω is the angular frequency.

Assume there is a layered structure of air (ε_0, μ_0 and σ_0) and isotropic lossy ground (ε_1, μ_1 and σ_1), as shown in Fig. 1. For conductors situated in air, both potentials $\boldsymbol{A}$ and ϕ can be expressed using the Green's functions [30], as follows:

$$\begin{aligned}\boldsymbol{A}(r)&=\int\overline{\overline{\boldsymbol{G}}}_A(r,r')\cdot I(r')d\boldsymbol{l}'\\ \phi(r)&=\int K_\phi(r,r')\tau(r')dl'+\int C_\phi(r,r')\hat{z}\cdot I(r')d\boldsymbol{l}'\end{aligned} \tag{2}$$

where both $I(r')$ and $\tau(r')$ are the conductor current and line charge density at r' on the source conductor. $\overline{\overline{\boldsymbol{G}}}_A$ is a dyadic Green's function for vector potential $\boldsymbol{A}$, and has different components for current dipoles in three orthogonal directions. It is expressed as,

$$\begin{aligned}\overline{\overline{\boldsymbol{G}}}_A&=G_{xx}\hat{x}\hat{x}+G_{yy}\hat{y}\hat{y}+G_{zz}\hat{z}\hat{z}+G_{zx}\hat{z}\hat{x}+G_{zy}\hat{z}\hat{y}\\&=G_{tt}\hat{t}\hat{t}+G_{zz}\hat{z}\hat{z}+G_{zt}\hat{z}\hat{t}\end{aligned} \tag{3}$$

where $\hat{t}$ is the unit vector of a current dipole projected on the xy plane or the ground surface, and $G_{tt}=G_{xx}=G_{yy}$. In (2) K_ϕ is a scalar Green's function for electric potential. Note in [30] that a unique scalar Green's function does not exist for a current dipole orientated in the stratified media. A correction term C_ϕ arising from the z component of the current dipole is introduced so that the Lorentz's gauge, i.e., $\nabla\cdot\boldsymbol{A}(r)=-j\omega\mu_0\epsilon_0\phi(r)$, is satisfied. The expressions of these Green's functions and the correction term are given in Appendix A.

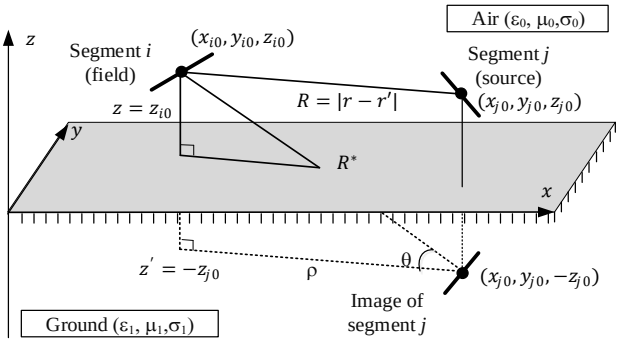

Fig. 1 Configuration of segments in the air-ground media

Divide the conductor into a set of short segments, and select two segments; field segment i and source segment j. Then substitute (2) into (1) and integrate (1) along the field segment. A set of potential equations yield, as follows:

$$\begin{aligned}\frac{s_i}{\sigma}J_i+\sum_j j\omega\int_{l_i}\int_{l_j}\overline{\overline{\boldsymbol{G}}}_A(r,r')\cdot d\boldsymbol{l}_i\cdot d\boldsymbol{l}'_j\,I_j&=\phi_n-\phi_m\\ \phi_n=\sum_k\int_{l_k}K_\phi(r,r')dl'_k\,\tau_k+\sum_j\int_{l_j}C_\phi(r,r')\hat{z}\cdot d\boldsymbol{l}'_j\,I_j&\end{aligned} \tag{4}$$

where J_i is the current density on the surface of segment i, and s_i is the length of segment i.

Let V be the average value of potential ϕ over a node segment, electrical circuit equations can be established, as follows:

$$\begin{aligned}Z_{si}I_i+\sum_j j\omega L_{ij}I_j&=V_n-V_m\\ V_n=\sum_k p_{nk}q_k+\sum_j c_{nj}I_j&\end{aligned} \tag{5}$$

where q_k is the total charge on segment k. Z_{si} is the surface impedance of the conductor, and can be expressed by

$$Z_{s,i}=\frac{J_i}{\sigma I_i}=-\frac{j\omega\mu}{2\pi R_a}\cdot\frac{J_0(R_a)}{J_1(R_a)} \tag{6}$$

for the circular conductor with conductivity σ and permeability μ_0 and radius a [32], and $R_a=\sqrt{-j\omega\mu\sigma}\,a$. $J_n(*)$ is the Bessel function of the 1st kind of order n. In (5) parameters L_{ij} and p_{nk} are the partial inductance and potential coefficient of segments, and c_{nj} is the correction coefficient. They are given by

$$\begin{aligned}L_{ij}&=j\omega\int_{l_i}\int_{l_j}\overline{\overline{\boldsymbol{G}}}_A(r,r')\cdot d\boldsymbol{l}'_j\cdot d\boldsymbol{l}_i\\ p_{nk}&=\frac{1}{s_n s_k}\int_{l_n}\int_{l_k}K_\phi(r,r')dl_k dl_n\\ c_{nj}&=\frac{1}{s_n}\int_{l_n}\int_{l_j}C_\phi(r,r')\hat{z}\cdot d\boldsymbol{l}'_j dl_n\end{aligned} \tag{7}$$

where s_i ($i=n,j\ or\ k$) is the length of segment i. By taking the time derivative of potential in (4), the capacitive current on the node in the frequency domain is obtained as,

$$I_{c,n}=j\omega q_n=\frac{1}{p_{nn}}j\omega V_n-\sum_k\frac{p_{nk}}{p_{nn}}I_{c,n}-\sum_j\frac{j\omega c_{nj}}{p_{nn}}I_j \tag{8}$$

Fig. 2 shows the equivalent circuit diagram for the equations given in (5) and (8). Both node voltage V_n and branch current I_i are two sets of unknowns in the equivalent circuit, which can be solved by a conventional circuit analysis tool.

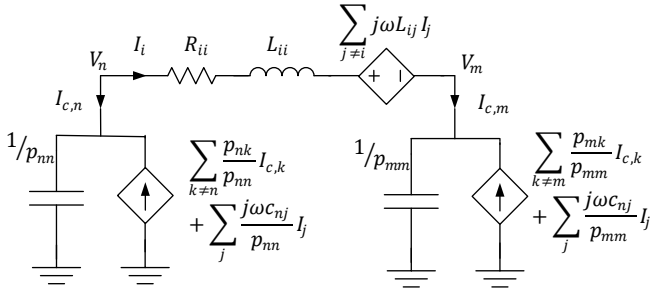

Fig. 2 Equivalent circuit of a line segment

It is noted in (3) and (7) that inductance L_{ij} contain a coupling element from a horizontal (source) segment to a vertical (field) segment, which does not exist in the traditional definition of inductance. This element is introduced purely due to the presence of the lossy ground, and is the correction term for mutual inductive coupling. However, vertical current segments do not have any inductive contribution to horizontal current segments, because of asymmetric matrix $\overline{\overline{\boldsymbol{G}}}_A$. This is one-way coupling. It is, however, noted that the vertical current segments do have a contribution to the node potential, as seen in (2).

When a current-carrying conductor penetrates into the ground, a medium different from the air, a second potential correction term [30] will arise in the expression of node potential given in (4). In case of thin wires, the node potential in (5) is revised to be,

$$V_n = \sum_k p_{nk} q_k + \sum_j c_{nj} I_j + \sum_{j^*} \frac{1}{j\omega} c^*_{nj*} I_{g,j*}$$
$$c^*_{nj*} = \frac{1}{s_n} \int_{l_n} K_\phi(r,r') dl_n \tag{9}$$

where $I_{g,j*}$ is the ground current in segment j* connected to the ground. Fig. 3 shows the revised equivalent circuit containing the segment connected to the ground. In the figure Z_g represents the equivalent circuit of the grounding grid [33-34].

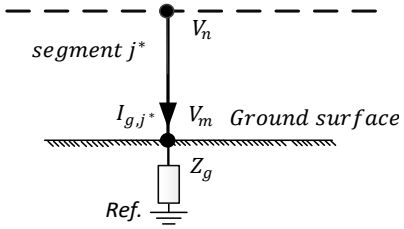

(a) A line crossing over the ground surface

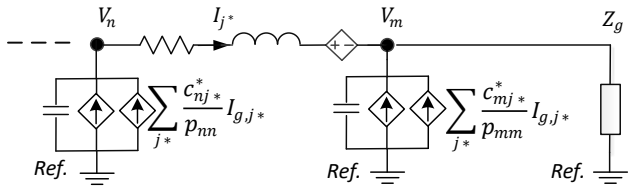

(b) Correction term arising from the ground connection

Fig. 3 PEEC model of a wire structure connected to the ground

III. Evaluation of Circuit Parameters

A. General expressions of circuit parameters

Fig. 1 shows two arbitrary line segments i and j with direction cosines $(\cos\alpha_i, \cos\beta_i, \cos\gamma_i)$ and $(\cos\alpha_j, \cos\beta_j, \cos\gamma_j)$ together with the mirror image under the ground. Because both horizontal and vertical current dipoles have different Green's functions, inductance has to be calculated separately for these components. Assume Green's function of free space $G_0(r,r') = e^{-jk_0R}/R$, where free-space wavenumber $k_0 = \omega\sqrt{\mu_0\epsilon_0}$ and $R = |r - r'|$. According to Appendix A, both partial inductance (external or mutual inductance) between field segment i and source segment j and coefficient of potential between field segment n and source segment m are expressed from (7) and (9) as,

$$L_{ij} = \frac{\mu_0}{4\pi}\left[\int_{l_i}\int_{l_j} G_0(r,r')dl_i dl'_j g_a + \int_{l_i}\int_{l_j} U(r,r')dl_i dl'_j g_b - \int_{l_i}\int_{l_j} N(r,r')dl_i dl'_j g_c + \int_{l_i}\int_{l_j} W(r,r')dl_i dl'_j g_d \cos\xi_{ij}\right]$$
$$p_{nm} = \frac{1}{4\pi\varepsilon_0 s_n s_m}\left[\int_{l_n}\int_{l_m} G_0(r,r')dl_n dl'_m + \int_{l_n}\int_{l_m} M(r,r')dl_n dl'_m\right]$$
$$c_{nj} = \frac{\mu_0}{4\pi}\frac{1}{s_n}\int_{l_n}\int_{l_j} C(r,r')dl_n dl'_j \cos\gamma_j$$
$$c^*_{nj*} = \frac{1}{4\pi\varepsilon_0}\frac{1}{s_n}\int_{l_n}\left(G_0(r,r') + M(r,r')\right)dl_n \tag{10}$$

where functions U, N, W, M and C in (10) are the Sommerfeld integrals given in Appendix A. They can be expressed as $X_0\, e^{-jk_0R^*}/R^*$, where X_0 is the normalized coefficient and $R^* = \sqrt{\rho^2 + (z+z')^2}$. R^* is the distance between the field segment in air and the mirror image of the source segment, as illustrated in Fig. 1. X_0 is evaluated by using the real-axis direct integration method [35], and is tabulated at each frequency.

In (10) coefficients g_x ($x = a, b, c$ and d) are given by

$$g_a = \cos\alpha_i \cos\alpha_j + \cos\beta_i \cos\beta_j + \cos\gamma_i \cos\gamma_j$$
$$g_b = \cos\alpha_i \cos\alpha_j + \cos\beta_i \cos\beta_j$$
$$g_c = \cos\gamma_i \cos\gamma_j$$
$$g_d = \cos\gamma_j \sqrt{1 - \cos\gamma_i^2}$$

Both g_a and g_b in (10) project one segment onto another one in 3D space and on the ground surface, respectively. Both g_c and g_d project respectively two segments onto the z axis, and one onto the z axis and another one onto the ground surface. ξ_{ij} is the angle on the ground surface between the t component of source segment j and the z component of field segment i, as shown in Fig. 4. It is given by

$$\cos\xi_{ij} = \frac{\Delta x\cos\alpha_j + \Delta y\cos\beta_j}{\sqrt{\Delta x^2 + \Delta y^2}\cdot\sqrt{1-\cos\gamma_j^2}} \tag{11}$$

It is found in (10) that mutual inductance is contributed by coupling (i) of two segments in free space, (ii) of components in z direction, (iii) of components in t directions and (iv) from the t component to the z component in the presence of a lossy ground. As the coupling from the z component to t component is missing in (10), inductance L_{ij} may not be equal to L_{ji}.

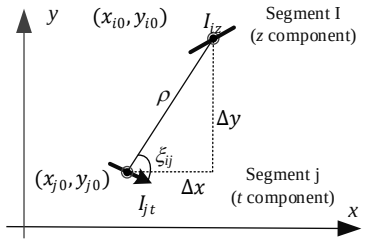

Fig. 4 Configuration of both t and z components on the xy plane

The inductance formula can be simplified for two segments either in parallel with or perpendicular to the ground surface. For cases of (a) two segments in parallel with the ground, (b) two segments perpendicular to the ground, and (c) one segment in parallel with and one perpendicular to the ground, inductances are expressed as

$$L_{ij,a} = \frac{\mu_0 g_a}{4\pi}\int_{l_i}\int_{l_j}\frac{e^{-jk_0R}}{R}dl_i dl'_j + \frac{\mu_0 g_b}{4\pi}\int_{l_i}\int_{l_j} U_0\frac{e^{-jk_0R^*}}{R^*}dl_i dl'_j$$
$$L_{ij,b} = \frac{\mu_0}{4\pi}\int_{l_i}\int_{l_j}\frac{e^{-jk_0R}}{R}dl_i dl'_j - \frac{\mu_0}{4\pi}\int_{l_i}\int_{l_j} N_0\frac{e^{-jk_0R^*}}{R^*}dl_i dl'_j$$
$$L_{ij,c} = \frac{\mu_0\cos\xi_{ij}}{4\pi}\int_{l_i}\int_{l_j} W_0\frac{e^{-jk_0R^*}}{R^*}dl_i dl'_j \tag{12}$$

where the 1st term in (12) for case a or b is the free-space inductance between two segments. Coefficient of potential exists in any two arbitrary segments including two perpendicular segments. It is expressed with the coefficient of potential in free space and the ground contribution, as follows:

$$p_{nm}=\frac{1}{4\pi\varepsilon_0 s_n s_m}\int_{l_n}\int_{l_m}\left[\frac{e^{-jk_0R}}{R}+M_0\frac{e^{-jk_0R^*}}{R^*}\right]dl_n dl'_m \quad (13)$$

These double-fold line integrals can be evaluated numerically, as values of the Sommerfeld integrals are obtained from the lookup tables.

B. *Circuit parameters for specific grounds*

As seen in Appendix A, kernels of the Sommerfeld integrals are explicit functions of TE/TM-mode reflection coefficients Γ^e and Γ^h according to (A5). They are determined by wavenumbers k_0 in air and $k_1=\omega\sqrt{\mu_1\epsilon_1}$ in ground. In case of perfectly conducting ground (PCG), $k_1^2\to -j\infty$, both reflection coefficients Γ^e and Γ^h approach -1. Sommerfeld integrals in (A4) can be then simplified, i.e., normalized coefficients $W_0=C_0=0$ and $U_0=N_0=M_0=-1$, as seen in Appendix A.

At extreme low frequency (LFG), i.e., $\omega\to 0$, reflection coefficients Γ^e and Γ^h respectively approach -1 and 0 according to (A5). Then coefficients of the Sommerfeld integrals can be simplified as well , as seen in Appendix A, i.e., $U_0=C_0=0$, $N_0=M_0=-1$ and $W_0=(sin\theta-1)/cos\theta$ where θ is defined in Fig.1. Table 1 summaries normalized coefficients of the Sommerfeld integrals for these two ground models. In these ground models the ground is substituted with the source images. Fig. 5(a) shows the images of current and charge as well as coupling for a perfectly conducting ground (PCG), and Fig. 5(b) shows those for the low-frequency ground (LFG), which is the approximation of a lossy ground. Appendix B shows the closed-form expressions of inductance and coefficient of potential for segments when $k_0R\ll 1$.

Table 1. Normalized coefficient of the Sommerfeld integrals in two models

Ground Model	U_0	N_0	W_0	M_0	C_0
PCG	-1	-1	0	-1	0
LFG	0	-1	$(sin\theta-1)/cos\theta$	-1	0

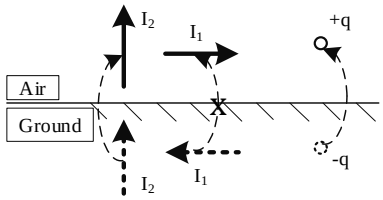

(a) Perfectly conducting ground (PCG model)

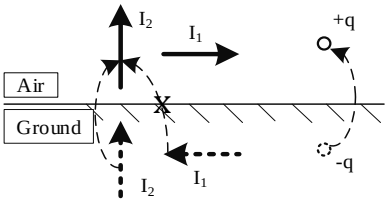

(b) Low-frequency ground (LFG model)

Fig. 5 Source current and charge and their images for two ground models:
"---->" represents the coupling from one element to another one
"-x->" means that the coupling in the model does not exist in another model

C. *Numerical evaluation of circuit parameters*

Inductance and coefficient of potential for four segments situated above a lossy ground have been calculated using the proposed method. Fig. 6 shows the configuration of four short segments. All the segments are 1 m in length with $h_1=h_3=1\ m$ and $h_2=h_4=10\ m$. Other parameters are listed in Table 2.

Table 2. Wire and Soil parameters used in the simulation

Wire parameters		Soil parameters	
Diameter (m)	Conductivity (S/m)	Conductivity (S/m)	Relative permittivity
0.005	5.8e8	1e-3	10

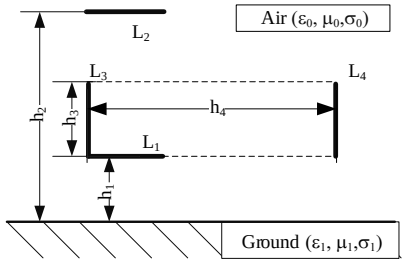

Fig. 6 Configuration of three segments for circuit parameter evaluation

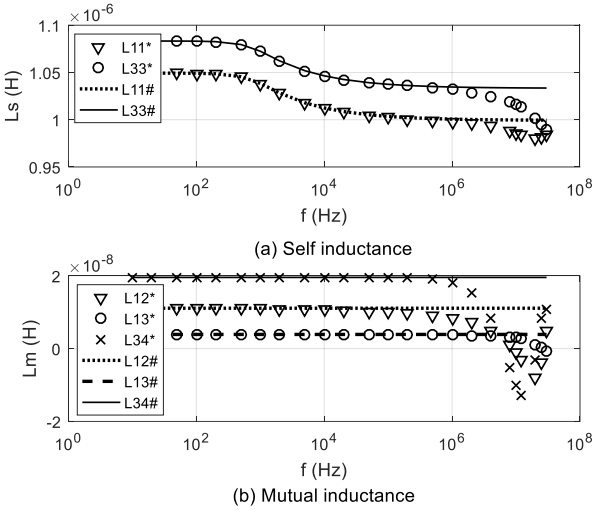

Fig. 7 Self and mutual Inductance among three segments (L*: calculated with the Sommerfeld integrals (LSG), L#: calculated with LFA formulas)

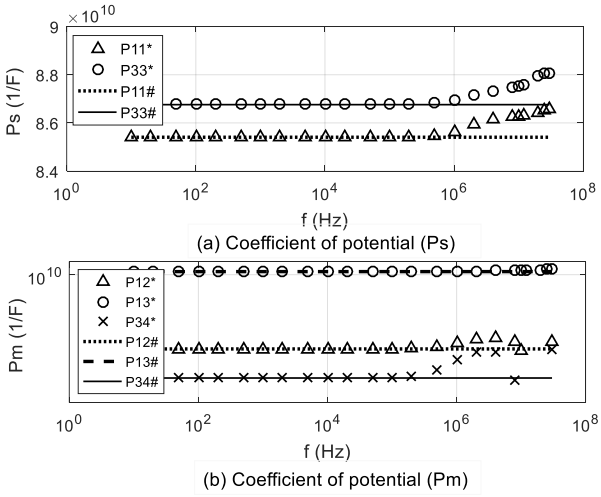

Fig 8. Coefficients of the potential of three segments (L*: calculated with the Sommerfeld integrals (LSG), L#: calculated with LFA formulas)

Fig. 7 shows the self and mutual inductance of these segments in the frequency range from 10 Hz to 25 MHz, calculated using the Sommerfeld integrals (LSG model). The inductance of segments calculated with LFG formulas is presented in the figure as well for comparison. Note that the self-inductance of a segment includes both internal and external components. Internal inductance is affected by its skin effect at 700 Hz or above, and is negligible at 100 kHz or above. It is found that the inductance calculated with the Sommerfield integrals (LSG) and LFG formulas match very well for the frequency up to 1 MHz. This indicates that LFG is a good approximation of the lossy ground (LSG) at low frequency. It is found that there is a discrepancy of mutual inductance L_{12} between two models at some frequencies less than 1 MHz. As mutual inductance is much less than self inductance, such difference would not cause significant errors in the transient analysis, as shown in the following sections. The mutual coupling between horizontal and vertical segments does exist, but the contribution is relatively small, compared with the coupling coefficient between parallel segments.

Fig. 8 shows self and mutual potential coefficients among three segments in the frequency range from 10 Hz to 25 MHz. These coefficient curves are calculated again with both the Sommerfeld integrals (LSG) and LFG formulas. It is noted that good agreements are observed for the frequency below 1 MHz. The lossy ground can be considered as the perfectly conducting ground no matter what orientation the segment has. When the frequency is greatest than 1 MHz, the effect of a lossy medium becomes significant and varies with increasing frequency.

IV. Comparison with NEC2 Codes

A comparison between the proposed PEEC model and numerical electromagnetic code NEC2 [28] was made in this section. Fig. 9 shows the configuration of an L-shape wire structure for comparison. The structure consists of two connected wires with a length of 18.3m for each, and is situated over a lossy ground at the height of $h = 1$ m. Other parameters are listed in Table 2. This wire structure is excited by a voltage source (1V with an internal resistance of 50 ohms) placed in the middle point of the horizontal wire, and currents on the wires are analyzed.

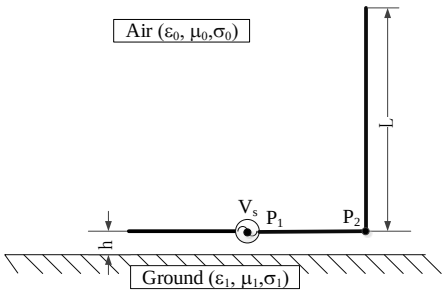

Fig. 9. Configuration of a wire structure for validation

In the PEEC simulation, each of these wires was divided into 61 elementary segments. Electrical circuit parameters, such as partial inductance and coefficient of potential among these segments were calculated using (10). Both segment current and node potential were analyzed using the procedure based on the modified loop analysis. Fig. 10 shows the frequency response of the currents at two points from 0.1 MHz to 25 MHz. Point P1 is located at the feeding point of the horizontal wire, and P2 is at the corner of the structure. The segment current at the corner would be affected significantly by the mutual inductance between two orthogonal wires.

Simulation of the currents in the wire structure was conducted again using NEC2. For the purpose of comparison, each of the wires in the structure was divided into 61 segments as well in the NEC2 model. The results are presented in Fig. 10 together with the PEEC results. It is found in the figure that both NEC2 and PEEC results match very well. The root mean square of the difference in percentage over the frequency range is less than 0.7%. The maximum difference is less than 1.4%. The simulation with 41 segments in each wire was performed again. It is found that the maximum difference is now increased to 3%.

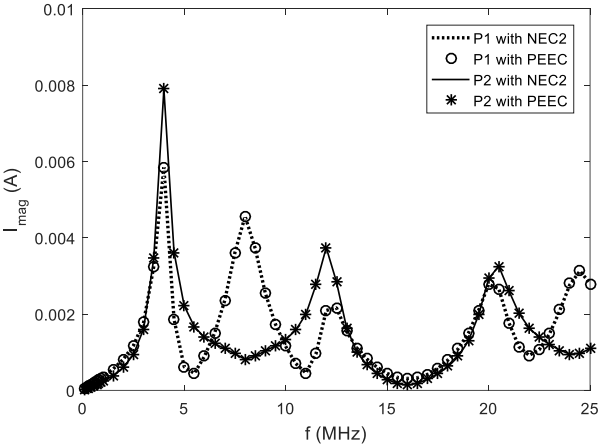

Fig. 10 Comparison of NEC2 and PEEC results

V. Computer Simulation of Transients in a Wire Structure

The computer simulation was also performed to analyze time-domain transient currents in wire structures situated above the same lossy ground. Fig. 11 shows the configuration of two 1 m x 1 m loops separated by a distance of 3 m. Other parameters are listed in Table 2. Loop A is excited by an impulse current source. Induced transient current is then generated in Loop B. In the simulation, the frequency-domain source current was first obtained by using the fast Fourier transform (FFT) technique. The induced current was then simulated with the proposed method in the frequency domain. Finally, the time-domain induced current was calculated by using the inverse FFT technique.

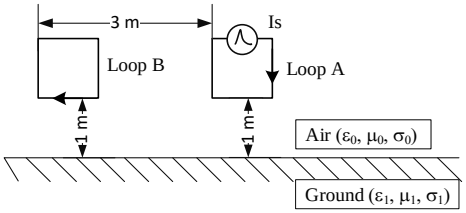

Fig. 11 Configuration of a wire structure for lighting transient simulation

In the simulation the impulse current was set to have the magnitude of 50 kA and the waveform of 0.25/100 μs. Three

different ground models were tested, i.e., perfectly conducting ground (PCG), lossy ground (LSG), low-frequency ground (LFG) — an approximation of the lossy ground. All the wires were divided into segments with a length of 0.1 m. Fig. 11 shows the induced current simulated with the proposed method for three ground models. It is found that the low-frequency ground model matches with the lossy ground model very well. The difference is generally less than 1.5%. However, there is a large difference between the lossy ground model and the perfectly conducting ground model. For comparison, the induced current calculated with the FDTD method [34] is presented in the figure as well. A good agreement is observed with the difference being less than 1.5%. In the FDTD model, the working volume is divided into $360 \times 200 \times 250$ cells. A non-uniform mesh technique is adopted. The cell size is 1 mm on the conductor, and increases to 100 mm gradually. The perfectly matched layer (PML) absorbing boundary conditions are applied to absorb unwanted wave reflections in six boundaries. The time step is defined as 1.92583e-13 s.

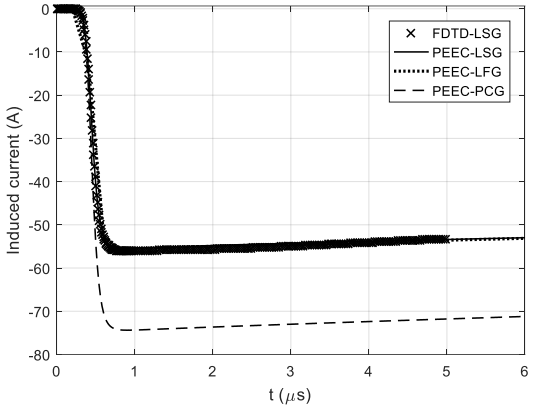

Fig. 12 Induced current in Loop B calculated by PEEC and FDTD methods

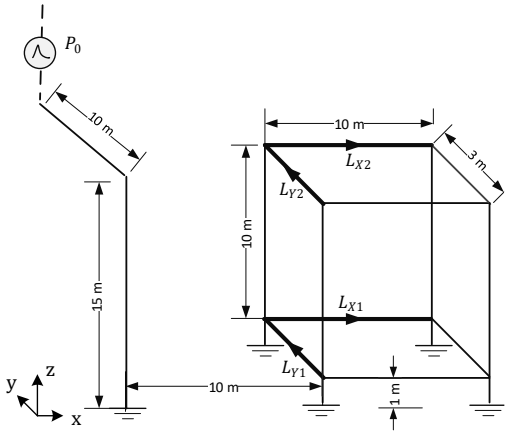

Fig. 13 Configuration of a wire structure for lighting transient simulation

The computer simulation was performed as well in a grounded structure, as shown in Fig. 13. Fig. 13 shows the configuration of a wire structure struck by lightning. Wire and ground parameters are listed in Table 2. The return stroke current is represented by a current source at Point P_0 on a vertical wire. The return stroke current has a magnitude of 50 kA and the waveform of 0.25/100 μs. A similar wire representing the lightning channel is extended upwards from Point P_0. In the simulation, the wires were divided into segments with a length of 1 m. Induced transient currents were simulated in the wire structure 10 m away from the vertical wire, i.e., the induced currents in the lines close to the ground (Lx1 and Ly1) and the lines away from the ground (Lx2 and Ly2).

Fig. 14(a) shows the simulated lightning transient currents in two y-dir. branches of the wire structure under a lightning stroke. It is found that the results obtained from both LSG and LFG match very well at the wave tail. The error of the wavefront is relatively large. This is because the low-frequency ground is an approximation of the lossy ground at the low frequency. The model of perfectly conducting ground, however, creates a much large error for the current in the branch close to the ground surface. It is noted again that PCG does not produce a bipolar waveform in the early time period. Fortunately, the difference is significantly reduced if the wire is far away from the ground surface, i.e., 11 m above the ground, as shown in Fig. 14(a). Fig. 14(b) shows the simulated lightning transient currents in two x-dir. branches of the structure. Similar results can be observed. The induced currents obtained with LFG match with those with LSG, no matter where the wire is located. There is a slight distortion in the wavefront in the LFG results. The induced current calculated with PCG is not as good as that with LFG.

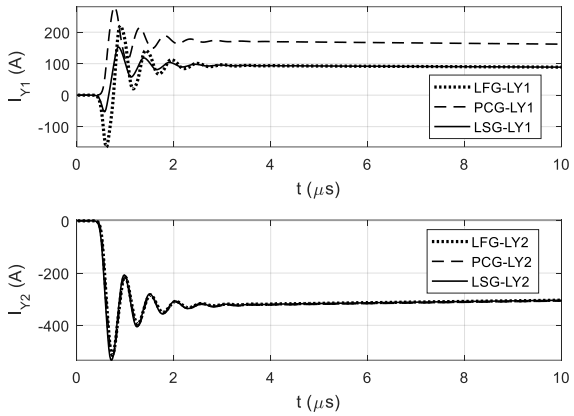

(a) Induced currents in two y-dir. branches

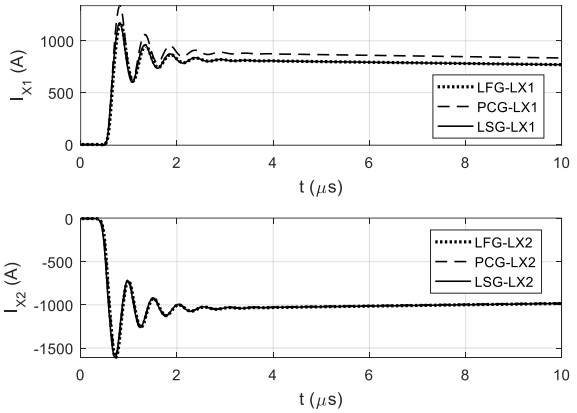

(b) Induced currents in two x-dir. branches

Fig. 14 Lightning transient currents in a wire structure under the lightning stroke current of 0.25/100 μs

The simulation was performed again when the lightning return stroke current has a waveform of 10/350 μs. Fig. 15

shows simulated lightning transient currents at the same locations as those shown in Fig. 14. It is found that both LFG model and LSG model match very well for the entire curves. In this case, the 10/350 μs waveform contains low-frequency components only, and the LFG model is a perfect approximation of the lossy ground. Similar to the previous case, a large deviation of the transient current calculated using the PCG model is found in the branch close to the ground. The computation time for the simulation case shown in Fig. 13 was also recorded. It is (1) 3 hr 30 min 46 s using the LSG model (Sommerfeld integrals), (2) 42 s using the LFG model, or (3) 37 s using the PCG model using a PC with i7-4749 CPU @3.6GHz and 16GB RAM.

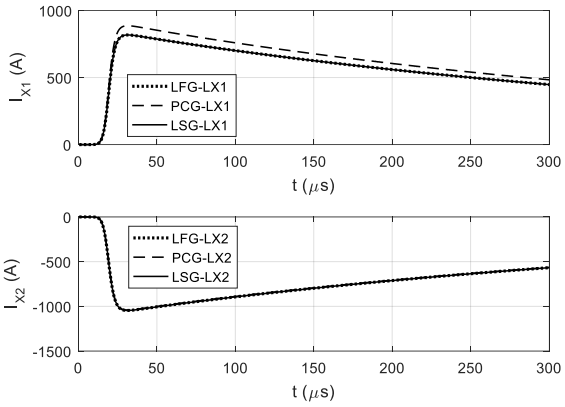

(a) Induced currents in two y-dir. Branches

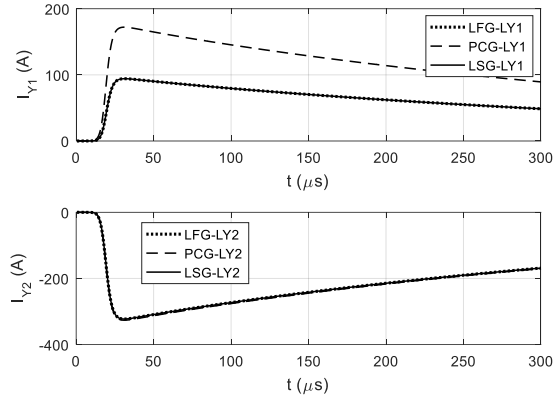

(b) Induced currents in two x-dir. branches

Fig. 15 Lightning transient currents in a wire structure under the lightning stroke current of 10/350 μs

VI. Conclusions

This paper presented a full-wave PEEC formulation for arbitrary-orientated conductors over a lossy ground. The equivalent circuit model of wires situated in air was derived for lightning transient analysis. Because of the presence of the lossy ground, correction terms were introduced in the circuit as current-controlled current sources. Circuit parameters are expressed with the Sommerfeld integrals, which are evaluated numerically by a direct axis integration method. The proposed model has been validated numerically using NEC2 and FDTD.

The low-frequency model of a lossy ground was derived directly from the Sommerfeld integrals, in which the ground is replaced the mirror image of source elements, similar to the perfectly conducting ground. All circuit parameters are frequency independent, and can be evaluated directly with analytical formulas. Simulation results show that the low-frequency model can represent the lossy ground very well as long as the frequency is lower than 1MHz. The hurdle in the time-domain simulation arising from the presence of a lossy ground is overcome.

Appendix A

Fig. 1 shows a layered structure of air (ε_0, μ_0 and σ_0) and isotropic lossy ground (ε_1, μ_1 and σ_1). According to [37-39], components of the Dyadic Green's function for magnetic vector potential $\boldsymbol{A}(r)$ are expressed by

$$\begin{aligned} G_{xx}(r,r') &= \mu_0/4\pi\left[G_0(r,r') + U(r,r')\right] \\ G_{zz}(r,r') &= \mu_0/4\pi\left[G_0(r,r') - N(r,r')\right] \\ G_{zt}(r,r') &= \mu_0/4\pi \cdot W(r,r') \end{aligned} \tag{A1}$$

the Green's function for electric scalar potential is given by

$$K_\phi(r,r') = 1/4\pi\varepsilon_0\left[G_0(r,r') + M(r,r')\right] \tag{A2}$$

and the correction term is given by

$$C_\phi(r,r') = \mu_0/4\pi \cdot C(r,r') \tag{A3}$$

In (A1-A3) U, N, W, M and C are the Sommerfeld integrals and are expressed by

$$\begin{aligned} U(r,r') &= S_0\left(\Gamma^h/j\beta_1\right) \\ N(r,r') &= S_0\left(\Gamma^e/j\beta_1\right) \\ W(r,r') &= S_1\left((\Gamma^e - \Gamma^h)/\lambda^2\right) \\ C(r,r') &= S_0\left((\Gamma^e - \Gamma^h)/\lambda^2\right) j\omega \\ M(r,r') &= S_0\left(\Gamma^e/j\beta_0\right) - S_0\left((\Gamma^e - \Gamma^h)/j\beta_0\lambda^2\right)k_0^2 \end{aligned} \tag{A4}$$

Sommerfeld integrals with kernel $f(\lambda)$ for field point (x, y, z) and source point (x', y', z') in air are defined as [37]

$$S_n(f) = \int_0^\infty f(\lambda) e^{-j\beta_0(z+z')} J_n(\lambda\rho)\lambda^{n+1} d\lambda \tag{A5}$$

where $\beta_i^2 = k_i^2 - \lambda^2$, imag $(\beta_i) \le 0$, and $k_i^2 = \omega^2\epsilon_i\mu_i - j\omega\sigma_i\mu_i$ $(i = 0, 1)$. Horizontal distance $\rho = \sqrt{\Delta x^2 + \Delta y^2}$. In the Sommerfeld integrals shown in (A4), both Γ^e and Γ^h are the reflection coefficients of TE and TM mode waves, and are given by

$$\begin{aligned} \Gamma^e &= \frac{k_0^2\beta_1 - k_1^2\beta_0}{k_0^2\beta_1 + k_1^2\beta_0} = \frac{\varepsilon_0\beta_1 - \varepsilon_1\beta_0}{\varepsilon_0\beta_1 + \varepsilon_1\beta_0} \\ \Gamma^h &= \frac{\beta_0 - \beta_1}{\beta_0 + \beta_1} \end{aligned} \tag{A6}$$

Sommerfeld integrals U, N, W, M and C are calculated with the direct real-axis integration [35]. Lookup tables of normalized coefficients of the Sommerfeld integrals were generated, and were used in the computer simulation. The computation time for generating five lookup tables with 123 x 34 entries in each table is 7.3 sec using a PC with i7-4749 CPU @3.6GHz and 16GB RAM.

These Sommerfeld integrals can be simplified under extreme cases. In case of perfectly conducting ground ($\sigma \to \infty$), k_1^2 is approximated by $-j\omega\sigma$ and approaches $-j\infty$. Both reflection coefficients Γ^e and Γ^h approach -1 according to (A6). With the identity of $\int_0^\infty (e^{-j\beta_0(z+z')}/j\beta_0) J_0(\lambda\rho)\lambda d\lambda = e^{-jk_0R^*}/R^*$ [40], they are approximated by

$$
\begin{aligned}
U = N &= S_0\left(\frac{-1}{j\beta_0}\right) = -\frac{e^{-jk_0R^*}}{R^*} \\
W &= 0 \cdot \lim_{\sigma\to\infty} \int_0^\infty e^{-j\beta_0 z} J_1(k_\rho\lambda) d\lambda = 0 \\
C &= \lim_{\sigma\to\infty} S_0\left(\frac{2(\beta_1-\beta_0)}{k_0^2\beta_1 + k_1^2\beta_0} j\omega\right) = S_0(0) = 0 \\
M &= \lim_{\sigma\to\infty} S_0\left(\frac{-1}{j\beta_0} - \frac{2k_0^2(\beta_1-\beta_0)}{(k_0^2\beta_1 + k_1^2\beta_0)j\beta_0}\right) = -\frac{e^{-jk_0R^*}}{R^*}
\end{aligned}
\tag{A7}
$$

where $R^* = \sqrt{\rho^2 + (z+z')^2}$. At extreme low frequency (LFG), i.e., $\omega \to 0$, ϵ_1 approaches $-j\infty$ and both β_0 and β_1 are approximated by $-j\lambda$. Then reflection coefficients Γ^e and Γ^h respectively approach -1 and 0, as illustrated below,

$$
\begin{aligned}
\Gamma^e &= \lim_{\omega\to 0}\left(\frac{\varepsilon_0\lambda - \varepsilon_1\lambda}{\varepsilon_0\lambda + \varepsilon_1\lambda}\right) = -1 \\
\Gamma^h &= \frac{\lambda - \lambda}{\lambda + \lambda} = 0
\end{aligned}
\tag{A8}
$$

The Sommerfeld integrals can be then approximated by

$$
\begin{aligned}
U &= 0 \cdot \lim_{\omega\to 0} \int_0^\infty \frac{e^{-j\beta_0(z+z')}}{j\beta_0} J_0(\lambda\rho)\lambda d\lambda = 0 \\
N &= \lim_{\omega\to 0} \int_0^\infty \frac{e^{-j\beta_0(z+z')}}{-j\beta_0} J_0(\lambda\rho)\lambda d\lambda = -\frac{1}{R^*} \\
W &= \lim_{\omega\to 0} \int_0^\infty \frac{e^{-j\beta_0(z+z')}}{-1} J_1(k_\rho\lambda) d\lambda = \frac{1}{R^*}\frac{\sin\theta - 1}{\cos\theta} \\
C &= \lim_{\omega\to 0} S_0\left(\frac{2(\beta_1-\beta_0)}{-\sigma\beta_0}\right) = 0 \\
M &= \lim_{\omega\to 0} S_0\left(\frac{-1}{j\beta_0} - \frac{2\varepsilon_0(\beta_1-\beta_0)}{(\varepsilon_0\beta_1 + \varepsilon_1\beta_0)j\beta_0}\right) = -\frac{1}{R^*}
\end{aligned}
\tag{A9}
$$

where θ is defined in Fig.1. The following identity [40] is applied in deriving the formula of W,

$$\int_0^\infty e^{-\lambda(z+z')} J_1(\lambda\rho) d\lambda = (1 - z/R^*)/\rho.$$

Appendix B

Inductance and coefficient of potential between two segments l and l' in air can be expressed with a double line integral, as seen in (12) and (13). In both LFG and PCG models, the double line integral can be expressed explicitly with a closed-form formula when $k_0 R \ll 1$ [41-42], as follows:

$$T_0 = \int_l \int_{l'} \frac{1}{R} dl dl' = \sum_{i,j=1,2} (-1)^{i+j} T_{ij} \tag{B1}$$

where, for parallel segments shown in Fig. B1(a)

$$T_{ij} = R_{ij} - \Delta u_{ij} \ln(\Delta u_{ij} + R_{ij})$$

for perpendicular segments shown in Fig. B1(b)

$$T_{ij} = \Delta u_{ij} \ln(\Delta u_{ij} + R_{ij}) + \Delta v_{ij} \ln(\Delta v_{ij} + R_{ij}) - \Delta w_{ij} \tan^{-1}\left(\frac{\Delta v_{ij}\Delta u_{ij}}{\Delta w_{ij} R_{ij}}\right)$$

In (B1) $R_{ij} = \sqrt{u_{ij}^2 + v_{ij}^2 + w_{ij}^2}$, $\Delta u_{ij} = u_i - u_j'$, $v\Delta_{ij} = v_i - v_j'$ and $\Delta w_{ij} = w_i - w_j'$ where u (u'), v (v') and w (w') are the coordinates of the end of field (source) segment l (l') in the Cartisian coordinate system. For two arbitrarily-orientated segments other than in Fig. B1, the double-line integral can be evaluated by a closed formula given in [41-42].

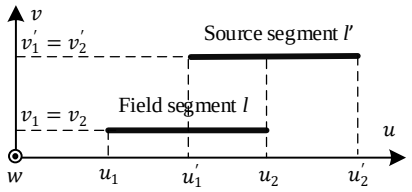

(a) Two parallel segments

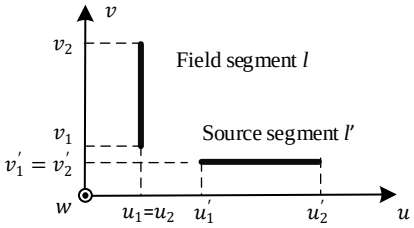

(b) Two perpendicular segments

Fig. B1 wire configuration for parameter calculation in air

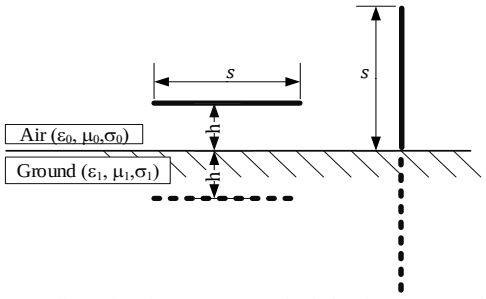

Fig. B2 Wire configuration for parameter calculation in two ground models ($s \gg h$ and $\gg a$)

Table B Self inductances and self potential coefficients of short wires above the ground ($s \gg h, s \gg a$)

Ground Model		Inductance	Coefficient of potential
Horizontal wire	PEC	$\frac{\mu_0 s}{2\pi}[\ln\left(\frac{2h}{a}\right)]$	$\frac{1}{2\pi\epsilon_0 s}[\ln\left(\frac{2h}{a}\right)]$
	LFG	$\frac{\mu_0 s}{2\pi}[\ln\left(\frac{2h}{a}\right)]$	$\frac{1}{2\pi\epsilon_0 s}[\ln\left(\frac{2h}{a}\right)]$
Ground Model		**Inductance**	**Coefficient of potential**
Vertical wire	PEC	$\frac{\mu_0 s}{2\pi}[\ln\left(\frac{4s}{a}\right) - 1]$	$\frac{1}{2\pi\epsilon_0 s}[\ln\left(\frac{s}{a}\right) - 1]$
	LFG	$\frac{\mu_0 s}{2\pi}[\ln\left(\frac{4s}{a}\right) - 1]$	$\frac{1}{2\pi\epsilon_0 s}[\ln\left(\frac{s}{a}\right) - 1]$

For short wires arranged in parallel with or perpendicular to the ground plane, the effect of the ground can be taken into consideration using the mirror image of the wire, as shown in

Fig. B2. Assume that segment length s is much greater than height h, and height h is much greater than segment radius a. Explicit formulas of inductance and coefficient of potential for these segments in two ground models can be obtained by using (B1). These formulas are presented in Table B.

ACKNOWLEDGMENT

The work leading to this paper was supported by grants from the Research Grants Council of the HKSAR (Project No. 15203815E and 15210018E).

REFERENCES

[1] P. R. Clayton, *Analysis of multiconductor transmission lines*, Hoboken, N.J.: Wiley-Interscience, IEEE Pres 2008.

[2] F. Rachidi, C.A. Nucci, M. Ianoz and C. Mazzetti, "Influence of a lossy ground on lightning-induced voltages on overhead lines," *IEEE Trans. on EMC*, vol. 38, vo. 3, pp.250-264, Aug. 1996

[3] C. D. Taylor, R. S. Satterwhite and C.W. Harrison, "The response of a terminated two-wire transmission line excited by a nonuniform electromagnetic field," *IEEE Trans. on AP*, vol.13, no.6, pp.987-989, 1965.

[4] A. K. Agrawal, H. J. Price, and S. H. Gurbaxani, "Transient response of multiconductor transmission lines excited by a nonuniform electromagnetic field," *IEEE Trans on EMC*, vol. 22, no. 2, pp. 119-129, 1980.

[5] P. Chowdhuri, "Lightning-induced voltages on multiconductor overhead lines," *IEEE Trans. on PWRD*, vol. 5 no. 2, pp. 658~667, 1990

[6] C. A. Nucci, M. Ianoz, and C Mazzetti, "Comparison of two coupling models for lightning-induced overvoltage calculations," *IEEE Trans. on PWRD*, vol. 10, no. 1, pp. 330-339, 1995

[7] V. Cooray, "Calculating lightning-induced overvoltages in power lines: A comparison of two coupling models," *IEEE Trans on EMC*, vol. 26, no 3, pp. 79-182, 1994

[8] S. Tkatchenko, F. Rachidi and M. Ianoz, "Electromagnetic field coupling to a line of finite length: Theory and fast iterative solutions in frequency and time domains," *IEEE Trans on EMC,* vol. 37, no. 4, pp. 509-518,1995

[9] A. E. Ruehli, "Equivalent circuit models for three-dimensional multiconductor systems," *IEEE Trans. Microw. Theory Tech*., vol. 22, no. 3, pp. 216–221, Mar. 1974

[10] A. Ruehli, Jan Garrett, and Clayton Paul. "Circuit models for 3D structures with incident fields," *in 1993 IEEE International Symposium on EMC*, Dallas, TX, Aug. 1993, pp. 28-32

[11] S. V. Kochetov, "Time- and frequency-domain modeling of passive interconnection structures in field and circuit analysis," Habilitation dissertation, Otto-von-Guericke-Univ. Magdeburg, Germany, 2008.

[12] J. Nitsch, F. Gronnwald, and G. Wollenberg, Radiating Nonuniform Transmission-Line Systems and the Partial Element Equivalent Circuit Method. Hoboken, NJ: Wiley, 2009.

[13] A. E. Ruehli, G. Antonini, and L. Jiang, Circuit Oriented Electromagnetic Modeling Using the PEEC Techniques. Hoboken, NJ: Wiley-IEEE Press, 2017.

[14] G. Antonini, S. Cristina and A. Orlandi, "PEEC modeling of lightning protection systems and coupling to coaxial cables," *IEEE, Trans. on EMC*, vol. 40, no. 4, pp.481, Nov. 1998

[15] A. Orlandi and F. Schietroma, "Attenuation by lightning protection system of induced voltages due to direct strikes to a building," *IEEE Trans. on EMC*, vol. 8, no. 1, pp. 43-50, 1996

[16] P. Yutthagowith, A. Ametani, N. Nagaoka and Y. Baba, "Application of the partial element equivalent circuit method to analysis of transient potential rises in grounding systems," *IEEE Trans. on EMC*, vol. 53, no. 3, pp726-736, 2011

[17] Q. B. Zhou and Y. Du, "Using EMTP for evaluation of surge current distribution in metallic gridlike structures," *IEEE Trans. on IA*, vol. 41, no. 4, pp1113-1117, 2005

[18] H. Chen, Y. Du and M. Chen, "Lightning transient analysis of radio base stations." *IEEE Trans on PWRD*, vol. 33, no. 5, pp. 2187-2197, 2018

[19] Hongcai Chen and Ya-ping Du, "Model of ferromagnetic steels for lightning transient analysis." *IET Science, Measurement & Technology*, vol. 12, no. 3, pp. 301-307, 2018

[20] Ruihan Qi, Y. Du and Mingli Chen, "Time-domain PEEC transient analysis for a wire structure above the perfectly conducting ground with the Incident Field From a distant lightning channel," *IEEE Trans. on EMC*, DOI: 10.1109/TEMC.2019.2925140.

[21] Chiu-Chih Chou and Tzong-Lin Wu, "Direct simulation of the full-wave partial element equivalent circuit using standard SPICE," IEEE Microwave Magzine, July 2019, pp. 22-34.

[22] Y. Dou and K.-L. Wu, "A passive PEEC-based micromodeling circuit for high speed interconnection problems," IEEE Trans. on MTT., vol. 66, no. 3, pp. 1201–1214, Mar. 2018.

[23] J. Park, J. Lee, B. Seol, and J. Kim, "Fast and accurate calculation of system-level ESD noise coupling to a signal trace by PEEC model decomposition," IEEE Trans. MTT vol. 65, no. 1, pp. 50–61, Jan. 2017.

[24] N.H. Xia and Y.P. Du, "An efficient modelling method for 3-D magnetic plates in magnetic shielding," IEEE Trans on EMC, Vol. 56, No. 3, June 2014, pp. 608-614.

[25] Y. Du, SM Chen and J. Burnett, "Experimental and numerical evaluation of surge current distribution in buildings during a direct lightning stroke," *HKIE Transactions,* vol. 8, no. 1, pp.1-6, April 2001

[26] S.V. Kochetov, M. Leone and G. Wollenberg, "PEEC formulation based on dyadic Green's functions for layered media in the time and frequency domains," *IEEE Trans. on EMC*, vol. 50, no. 4, pp. 953-963, Feb. 2008

[27] Y. Du, "Circuit parameters of the vertical wires above the lossy ground in PEEC models," *IEEE Trans on EMC*, vol. 53, no. 4, pp871-879, 2012

[28] G.J. Burke *et al*., Numerical Electromagnetic Code (NEC), *Technical document 116:* Naval Ocean Systems Center, San Diego, 1980.

[29] R.E. Collin, *Field Theory of Guided Waves*, New York: McGraw-hill Company, 1960.

[30] K. A. Michalski and D. Zhang, "Electromagnetic scattering and radiation by surfaces of arbitrary shape in layered media, part I: theory," *IEEE Trans. on AP*, vol. 38 no. 3, pp. 335-344, 1990

[31] L. Xu, Y. Du and Q.B. Zhou, "The magnetic field and induced current arising from a cylindrical shell loop with an unbalanced current," *Electric Power System Research*, vol. 71, pp. 21-26, 2004

[32] S. Ramo, J.R. Whinnery and T. V. Duzer, *Fields and waves in communciatgion electronics*, New York: Wiley, Inc., 1994

[33] L. Grcev and F. Dawalibi, "An electromagnetic model for transients in grounding systems," *IEEE Trans. on PWDR*, vol. 5, no. 4, pp. 1773–1779, Oct. 1990.

[34] Hongcai Chen and Yaping Du, "Lightning grounding grid model considering both the frequency-dependent behavior and ionization phenomenon," *IEEE Trans on EMC*, vol. 61, no. 1, pp.157–165, Feb. 2019

[35] Y. Rahmat-Samii, R. Mittra and P. Parhami, "Evaluation of sommerfeld integrals for lossy half-space problems," *Electromagnetics,* vol. 1, pt. 1, pp.1-28, 1981

[36] Y. Du and Binghao Li and Mingli Chen, "The extended thin wire model of lossy round wire structures for FDTD simulations," *IEEE Trans. on PWRD*, Vol. 32, no. 2, pp. 2472-2480, 2017

[37] K.A. Michalski and J.R. Mosig, "Multilayered media Green's functions in integral equation formulations," *IEEE Trans. on AP*, vol. 45, no. 3, pp. 508-519, 1997

[38] Yaxun Liu, "Efficient simulation of EM response of dielectric objects in multilayered media," Ph.D thesis, University of Waterloo, Ontario, Canada, 2004

[39] K. A. Michalski, "On the scalar potential of a point charge associated with a time-harmonic dipole in a layered medium," *IEEE Trans. on AP*, vol. 35, no. 11, pp. 1299, 1987

[40] R.W.P. King, M. Owens and T.T. Wu, *Lateral electromagnetic waves: Theory and applications to communications, geophysical exploration, and remote sensing*, Hong Kong: Springer-Verlag, 1992

[41] P. R. Clayton, *Inductance: Loop and Partial*, Hoboken, N.J.: John Wiley & Sons, 2010

[42] F. W. Grover, *Inductance Calculations: working formulas and tables*, Research Triangle Park, N.C.: Instrument Society of America, 1973